The Sunyaev-Zel'dovich Effect Spectrum of Abell 2163

S. J. LaRoque[1], J. E. Carlstrom[1], E. D. Reese[1], G. P. Holder[1], W. L. Holzapfel[2], M. Joy[3], and L. Grego[4]

ABSTRACT

We present an interferometric measurement of the Sunyaev-Zel'dovich effect (SZE) at 1 cm for the galaxy cluster Abell 2163. We combine this data point with previous measurements at 1.1, 1.4, and 2.1 mm from the SuZIE experiment to construct the most complete SZE spectrum to date. The intensity in four wavelength bands is fit to determine the Compton y-parameter (y_0) and the peculiar velocity (v_p) for this cluster. Our results are $y_0 = 3.56^{+0.41+0.27}_{-0.41-0.19} \times 10^{-4}$ and $v_p = 410^{+1030+460}_{-850\ -440}$ km s^{-1} where we list statistical and systematic uncertainties, respectively, at 68% confidence. These results include corrections for contamination by Galactic dust emission. We find less contamination by dust emission than previously reported. The dust emission is distributed over much larger angular scales than the cluster signal and contributes little to the measured signal when the details of the SZE observing strategy are taken into account.

Subject headings: galaxies: clusters: individual (Abell 2163) — Sunyaev-Zel'dovich Effect — cosmic microwave background — techniques: interferometric

1. INTRODUCTION

The thermal Sunyaev-Zel'dovich effect (SZE) is a spectral distortion in the Cosmic Microwave Background (CMB) which results from the inverse Compton scattering of low-energy CMB photons by thermally distributed hot electrons in massive clusters of galaxies. The thermal SZE manifests itself as an increment in the Wien part of the CMB spectrum and a decrement in the Rayleigh-Jeans part of the spectrum (Sunyaev & Zel'dovich 1972), with a crossover wavelength of ~ 1.38 mm. There is also a kinetic SZE, caused by the bulk radial motion of the cluster with respect to the CMB rest frame. This effect shifts the CMB Planck spectrum to a slightly lower (higher) temperature for positive (negative) peculiar velocities where positive is defined as motion away from the observer.

[1]Department of Astronomy and Astrophysics, University of Chicago, Chicago, IL 60637

[2]Department of Physics, University of California, Berkeley, CA 94720

[3]Department of Space Science, SD50, NASA Marshall Space Flight Center, Huntsville, AL 35812

[4]Harvard-Smithsonian Center for Astrophysics, 60 Garden Street, Cambridge, MA 02138

In this paper, we present a recent 1 cm interferometric detection of the SZE in the cluster Abell 2163, obtained with the BIMA and OVRO arrays. We combine this measurement with a previous result from the Sunyaev-Zel'dovich Infrared Experiment (SuZIE), a six element bolometer array (Holzapfel et al. 1997a, hereafter H1997a) on the 10.4 m Caltech Submillimeter Observatory. The SZE in Abell 2163 was also observed by Diabolo, a two element bolometer array mounted on the IRAM 30 m telescope (Desert et al. 1998), and their result is included in Table 1. The measurement has considerable uncertainty and carries very little weight in the spectral fit relative to the SuZIE data. Due to the complication of estimating the effects of systematics on the Diabolo measurement, we have chosen to exclude it from our spectral fit. Thus, combining the four measurements from SuZIE and OVRO/BIMA, we construct the SZE spectrum and use it to determine the central Compton y-parameter and constrain the radial peculiar velocity of the cluster. We also address the concern that Galactic dust along the line of sight to the cluster may be a significant contaminant in the SuZIE bands (Lamarre et al. 1998). Using data from the Infrared Space Observatory (*ISO*) and the Infrared Astronomical Satellite (*IRAS*) we determine the level of dust contamination in the SuZIE measurements.

In §2, we describe our observations, data reduction, and dust analysis. In §3 we describe the theoretical model for the SZE spectrum and present the results of fitting our data to this model; we also consider several systematic uncertainties affecting the fit. All uncertainties are quoted at the 68% confidence level unless otherwise specified.

2. OBSERVATIONS AND DATA REDUCTION

The 1 cm observations were carried out at the Berkeley Illinois Maryland Association (BIMA) millimeter array and the Owens Valley Radio Observatory (OVRO) millimeter array during the summers of 1996, 1997, and 1998. The telescopes were outfitted with centimeter-wavelength receivers specifically designed to detect the SZE in distant galaxy clusters (Carlstrom et al. 1996). The receivers use cooled high electron mobility transistor (HEMT) amplifiers (Pospieszalski et al. 1995) sensitive to radiation between 0.83 and 1.15 cm with typical receiver temperatures in the range 11–20 K. Typical system temperatures (scaled to above the atmosphere) for the Abell 2163 observations range between 45 and 55 K.

We observed Abell 2163 at OVRO in 1996 and 1998 for a total of 37 hours with six 10.4 m telescopes providing a $4'.2$ FWHM primary beam; we used two 1 GHz wide bands centered at 1.0 cm and 1.05 cm. This cluster was observed at BIMA in 1996, 1997 and 1998 for 11 hours with nine 6.1 m telescopes providing a $6'.6$ FWHM primary beam; we used an 800 MHz bandwidth centered at 1.05 cm. At both observatories, we interleaved cluster measurements with observations of the radio point source 1549+026 (3.60 ± 0.01 Jy) every 25 minutes to monitor system gains, and we used Mars for our absolute flux calibration (Grego et al. 2000). We reduced the data using the MIRIAD software package (Sault et al. 1995) at BIMA and the MMA package (Scoville et al. 1993) at OVRO. In all observations, we flagged data from baselines where one telescope was shadowed by another, data that were not bracketed in time by observation of a phase calibrator, and data showing evidence of poor atmospheric coherence or spurious correlations. Figure 1 shows a deconvolved SZE image of Abell 2163 constructed from BIMA data. SZE images are produced with the software package DIFMAP (Pearson et al. 1994). In Figure 1 we have applied a Gaussian taper with a half power radius of 1.5 kλ to the *u-v* data. A bright point source has been removed from the image in Figure 1; see §2.1 for more details.

An interferometer measures the Fourier transform of the sky brightness, hence we fit a model to the data in the Fourier plane where the noise characteristics and spatial filtering of the interferometer are well understood. The model is constructed in the image plane, multiplied by the primary beam of the telescope, then Fourier transformed to the conjugate plane, known as the *u-v* plane, where it is compared with the data.

We model the cluster gas as a spherical isothermal-β model (Cavaliere & Fusco-Femiano 1978), where the SZE intensity change is given by

$$\Delta I_\nu(\theta) = \Delta I_{\nu 0}\left(1+\frac{\theta^2}{\theta_c^2}\right)^{(1-3\beta)/2}. \qquad (1)$$

Here $\Delta I_{\nu 0}$ is the central SZE decrement/increment at frequency ν, θ_c is the angular core radius of the cluster, and β is a power law index. We adopt the model shape parameters $\theta_c = 1'.20 \pm 0'.11$ and $\beta = 0.616 \pm 0.031$ from an analysis of *ROSAT* X-ray data (Holzapfel et al. 1997b, hereafter H1997b). With these shape parameters we find $\Delta I_{30} = -0.048 \pm 0.006$ MJy sr^{-1} (corresponding to a CMB temperature decrement $\Delta T_{\rm CMB} = -1780 \pm 210$ μK) where ΔI_{30} is the SZE decrement at 30 GHz. The statistical uncertainty in the central decrement is determined by varying ΔI_{30} while keeping the shape parameters fixed; all other parameters are free to assume their best-fit values. The uncertainties in θ_c and β quoted above lead to an additional 0.001 MJy sr^{-1} uncertainty on the 1 cm decrement.

The 1 cm decrement and combined statistical uncertainty are listed in Table 1, which also contains all spectral SZE data for this cluster available to date. The SuZIE $\Delta I_{\nu 0}$ values are from fits to the SuZIE data using the average of the measured spectral responses of the individual channels. The $\Delta I_{\nu 0}$ value from the Diabolo experiment is from Desert et al. (1998). As the table indicates, we have made small corrections in the SuZIE bands to account for dust contamination along the line of sight to the cluster. These corrections are described in more detail in §2.2.

2.1. Radio Point Sources

Point sources are identified in DIFMAP using a high-resolution map produced with data from baselines 20 meters and longer. We find one point source in the Abell 2163 data offset $-40''$ in RA and $16''$ in declination from the SZE pointing center, a position consistent with that of a variable radio source with an inverted spectrum detected by the VLA (M. Birkinshaw 2001, private communication) at 2 cm and 6 cm. The point source has been removed from the image in Figure 1.

The flux and position of the detected point source is jointly fit with the SZE decrement, but we must consider the uncertainty in the decrement introduced by point sources in the field with flux densities below our detection threshold. Such a point source near the cluster SZE center would cause us to underestimate the magnitude of the decrement, whereas a point source in a beam sidelobe could lead to an overestimate. To determine the resulting uncertainty we have randomly added point sources to the data as follows. Progressing in steps of 1 μJy, we choose a Poisson deviate of the expected number of point sources at each flux density. We add sources to the field accordingly out to a radius of $5'$, well past the half power point of the BIMA beam where faint point sources should have a negligible effect on the decrement. After reaching our 3σ flux density limit, we refit the SZE model without accounting for the added point sources.

To determine the number of point sources expected at each flux density, we first determine a point source number count versus flux density relationship of the form

$$dn/dS \propto S^{-\alpha} \text{ mJy}^{-1} \text{ arcmin}^{-2} \tag{2}$$

from our sample of 41 clusters observed at BIMA, where n is the number density of point sources and S is their flux density. We find that the distribution of sources beyond $10''$ from cluster centers agrees well with the expected distribution from a larger sample of point sources at 31 GHz (C. Pryke 2002, private communication). Inside $10''$, however, we detect nearly 30 times more point sources than expected due to the strong contribution of cluster cD galaxies. We therefore exclude the inner $10''$ of the map when selecting point sources to construct dn/dS and address the issue of central point sources in more detail below. We choose $240''$ as an outer limit in selecting point sources as it is a good trade-off between encompassing a large number of detected sources and allowing a low beam-corrected flux density threshold. We use only point sources with beam-corrected flux densities greater than 2 mJy, since a 2 mJy point source would have a beam-attenuated flux density of 0.75 mJy at $240''$ and 0.75 mJy is a good fiducial 3σ threshold for all 41 maps. Lastly, we assume the power law index determined from the Pryke sample, $\alpha = 2.4$, in Equation (2). Solving for the normalization, we find

$$dn/dS = 2.0 \times 10^{-2} \left(\frac{S}{\text{mJy}}\right)^{-2.4} \text{ mJy}^{-1} \text{ arcmin}^{-2}. \tag{3}$$

We then randomly distribute point sources according to this empirical relationship, starting from a flux density of 10 μJy (tests of the Monte-Carlo showed that starting at a lower flux density has a negligible effect on the decrement) up to a flux density of 300 μJy, corresponding to the 3σ limit of the more sensitive OVRO Abell 2163 data. The resulting distribution of best-fit decrements is nearly Gaussian and centered at the original decrement with a standard deviation of 0.002 MJy sr^{-1}. We adopt this as the statistical uncertainty due to randomly distributed undetected point sources, and it has been combined in quadrature with the other statistical uncertainties in Table 1.

We attempt to estimate the uncertainty from undetected point sources a second way, using information on the distribution of point sources in the field from observations at longer wavelengths. Sources with flux densities greater than ~ 2 mJy at 21 cm appear in the NVSS catalog (Condon et al. 1998). The catalog contains four point sources within $240''$ of Abell 2163 that we do not detect in our 1 cm observations. Searching the 100 μJy rms OVRO map at the positions of these sources, we find no evidence of emission from three of the four; their positions correspond to signals at the 0.2σ, -0.4σ, and -1σ levels. The fourth, however, displaced $30''$ in RA and $-127''$ in declination from the map center, corresponds to a 2σ signal in the OVRO map. We do not marginalize over the fluxes of all four sources because of the loss of degrees of freedom in the fit, but marginalizing over the 2σ source we find no change in either the decrement or the uncertainty in the decrement, which is dominated by the noise in the map.

To account for the fact that on-center point sources are statistically more common we place a point source model at the estimated position of Abell 2163's bright central galaxy (RA $16^{\rm h}15^{\rm m}49^{\rm s}.0$, Dec $-6°8'42''.7$ from Digitized Sky Survey) and marginalize over its flux. The new best-fit decrement is -0.049 MJy sr^{-1}, an increase in magnitude of just 0.001 MJy sr^{-1} from the original decrement. The new decrement falls easily within the 68% uncertainty of the original; we revisit this result when we discuss systematic uncertainties (§3.1).

2.2. Analysis of Dust Emission

Lamarre et al. (1998) (hereafter L1998) determined that IR cirrus flux is a non-negligible contaminant in the three SuZIE bands by including submillimeter data from the PRONAOS balloon experiment (Serra 1998) in their fit to the SuZIE and Diabolo data,. They accounted for dust by fitting to a combined SZE-spectral model and modified blackbody model, and found that removing the dust signal changed $\Delta I_{\nu 0}$ significantly. Specifically, they found that the 1.1 mm signal shrinks by 0.051 MJy sr^{-1} to 0.236 MJy sr^{-1}, the 1.4 mm signal changes by 0.018 MJy sr^{-1} to -0.124 MJy sr^{-1}, and the 2.1 mm band changes by 0.004 MJy sr^{-1} to -0.387 MJy sr^{-1}. L1998 assumed in their analysis that the SuZIE scan pattern is identical to the PRONAOS chopping scheme. However, PRONAOS performed a $6'.2$ chop at constant elevation (see L1998 for details) while SuZIE uses a drift scan at constant declination (H1997b). Thus, the experimental filters are different and will not necessarily detect the same dust signal.

To better estimate the level of dust contamination in the high frequency SuZIE channels, we have applied the SuZIE observing scheme to extrapolated dust maps at the SuZIE wavelengths. The expected dust contamination is listed in Table 2 and the dust-corrected SuZIE measurements are given in Table 1. Here we describe the procedure.

For clarity, we summarize the map construction procedures as applied to the 1.1 mm band; the 1.4 mm and 2.1 mm procedures are identical. The 1.1 mm dust map is created by extrapolating from three existing dust maps centered on Abell 2163; *ISO* maps at 90 μm and 180 μm, and an

IRAS map at 100 μm. We extract a $15' \times 1'.75$ central region from each dust map, consistent with the area of the SuZIE scans. We then smooth each map to a resolution consistent with the SuZIE beam size ($1'.75$), taking into account the intrinsic resolution of the IRAS and ISO experiments. We use a fiducial pixel to pixel uncertainty of 0.2 MJy sr^{-1} (cf. Beichman et al. 1988) for the *IRAS* map; for the *ISO* maps, we adopt the values estimated in L1998 of 0.14 MJy sr^{-1} and 0.18 MJy sr^{-1} at 90 and 180 μm, respectively. For each *ISO* map, we then bin the $0'.25$ pixels into $0'.75$ pixels, consistent with binning performed in the SuZIE analysis. For each new $0'.75$ pixel, we take the average of the original three $0'.25$ pixels as the intensity. The *IRAS* pixels are roughly twice the size of the binned *ISO* pixels, so we linearly interpolate to estimate the intensity of interleaved pixels, which we artificially add to the *IRAS* map. We then fit a modified blackbody to these dust maps at each pixel position; since we have three dust maps, each fit is to three data points, or one "pixel triplet". This allows us to extrapolate the intensities out to 1.1 mm. We fit a modified blackbody of the form

$$F_d \propto \frac{\nu^{3+\gamma}}{e^{h\nu/kT_d} - 1}, \tag{4}$$

where γ is the spectral index, T_d is the dust temperature, and we normalize the model with the dust flux at 180 μm, $F_d(180)$. Following L1998, we fix the spectral index at $\gamma = 2$. Upon fitting each dust pixel triplet to this model, we find $F_d(180)$ in the range 25.1 to 26.1 MJy sr^{-1} and T_d in the range 21.3 to 21.9 K over all triplets. We then use each triplet's best fit $F_d(180)$ and T_d with Gaussian error propagation to extrapolate the intensity at that position and create our 1.1 mm dust map.

After repeating this process at 1.4 and 2.1 mm, we perform the simulated scan following the detailed discussion of SuZIE's instrumental specifications and observing scheme in H1997b. In our simulation we scan across the $0'.75$ pixels of the dust maps in the direction of increasing right ascension (RA). For each pixel along the scan, we record the difference between its intensity and that of the pixel advanced $4'.6$ in RA; pixel-to-pixel uncertainties are combined in quadrature. This procedure is equivalent to SuZIE allowing the sky to drift overhead with the earth's rotation and recording the difference in signal between two bolometer array elements separated by $4'.6$ on the sky. We do not treat SuZIE's $2'.3$ "triple beam chop" here as it has little sensitivity to linear changes in brightness across the sky and therefore is less sensitive to dust; the results presented here serve as an upper limit to the dust contribution (see H1997b for more details). Our simulation thus creates "differenced" maps of the dust brightness.

We perform one-dimensional χ^2 fits in the parameter $\Delta I_{\nu 0}$ to the dust maps, fitting to a SuZIE-differenced β model with the pixel-to-pixel dust noise as our uncertainty. We use a Monte Carlo procedure and successively fit to 10^6 different realizations of the dust; in a single realization, each pixel has added to it some Gaussian-distributed amount of the pixel-to-pixel noise. The results of the Monte Carlo are highly Gaussian as expected; we thus take the most frequently returned $\Delta I_{\nu 0}$ as our best fit and those that enclose 68.3% of the returned $\Delta I_{\nu 0}$'s as our 1σ uncertainties. The results are shown in Table 2 and reflected in the last column of Table 1. We find a dust contamination level roughly seven times smaller than that reported in L1998, and small compared to the statistical uncertainties of the SZE measurements.

3. SZE SPECTRAL MODEL AND RESULTS

We have fit the dust-corrected SZE spectral data in Table 1 to a model which consists of both the thermal and kinetic SZE components. The thermal component, $\Delta I_{\rm T}$, can be written as

$$\Delta I_{\rm T} = I_0 y f(x)(1+\delta_{\rm T}) \tag{5}$$

where $x = h\nu/kT_{\rm CMB}$, $T_{\rm CMB} = 2.728$ K is the CMB temperature (Fixsen et al. 1996), $\delta_{\rm T}$ is a relativistic correction to the thermal effect good to fifth order in kT_e/m_ec^2 (Itoh et al. 1998), $I_0 \equiv 2(kT_{\rm CMB})^3/(hc)^2$, and

$$f(x) = \frac{x^4 e^x}{(e^x-1)^2}\left[\frac{x(e^x+1)}{e^x-1} - 4\right]. \tag{6}$$

The quantities h, k, and c are the Planck constant, Boltzmann constant, and speed of light, respectively. The quantity y is the Compton y-parameter, and is given by

$$y = \int \left(\frac{kT_e}{m_ec^2}\right) n_e \sigma_T dl, \tag{7}$$

where T_e is the electron temperature of the intracluster medium (ICM), m_e is the electron mass, n_e is the electron density, and σ_T is the Thomson scattering cross section. The Compton y-parameter is proportional to the pressure integrated along the line of sight (dl) through the cluster; we parameterize it in terms of a central value, which we denote y_0.

The kinetic component, $\Delta I_{\rm K}$, depends on both y and the radial peculiar velocity of the cluster, v_p, through the equation

$$\Delta I_{\rm K} = -(m_ec^2/kT_e) I_0 y \frac{v_p}{c} g(x)(1+\delta_{\rm K}) \tag{8}$$

where $g(x) = x^4e^x/(e^x-1)^2$ and $\delta_{\rm K}$ is a relativistic correction to the kinetic effect good to third order in kT_e/m_ec^2 (Nozawa et al. 1998). Corrections of order ${v_p}^2/c^2$ to the thermal and kinetic SZE are neglected since $v_p \ll c$. The total intensity is then the sum of the thermal and kinetic components,

$$\Delta I_\nu = \Delta I_{\rm T} + \Delta I_{\rm K}. \tag{9}$$

We perform a least squares fit to this model in the parameters y_0 and v_p assuming an ICM temperature T_e of $12.4^{+2.8}_{-1.9}$ keV from H1997b.

The resulting v_p and y_0 from the least squares fit to the four data points are $y_0 = 3.56 \pm 0.41 \times 10^{-4}$ and $v_p = 410^{+1030}_{-850}$ km s^{-1} with $\chi^2 = 0.8$ for two degrees of freedom. We compare this with the results of our fit to the SuZIE data only, $y_0 = 3.72 \pm 0.51 \times 10^{-4}$ and $v_p = 290^{+1020}_{-820}$ km s^{-1}. The addition of the 1 cm point improves the y_0 constraints by 18%. The constraints on v_p hardly change when the 1 cm point is included since constraints on peculiar velocity are dominated by the SuZIE data points which straddle the thermal SZE null.

Figure 2 shows the SZE spectrum generated from the fit to all four frequency bands. There is excellent consistency amongst all of the measurements. The data were obtained from independent experiments, each with its own telescope, detector, and observing strategy, operating at four different wavelengths. The consistency amongst the data attests to the reliability and accuracy with which the SZE is now being measured.

3.1. Systematic Uncertainties

In this section we address several additional sources of uncertainty in our spectral fits; the results of this analysis are summarized in Table 3.

We first consider the systematic uncertainty associated with the dust emission calculated in §2.2. When we alter the dust intensity at the 68% level, the spectral fit results change by $^{+0.00}_{-0.01} \times 10^{-4}$ for y_0 and $^{+0}_{-30}$ km s^{-1} for v_p. The dust uncertainties are sufficiently small as to have very little impact on the spectral fit results. We find a more significant change when we repeat the dust analysis with a smaller spectral index, γ. Finkbeiner et al. (1999) recently suggested based on fits to FIRAS data, that while $\gamma = 2$ is appropriate for wavelengths $\lesssim 600$ μm, the spectral index at longer wavelengths is closer to 1.5. Setting $\gamma = 1.5$ for the entire dust spectrum we find that y_0 increases by 0.02×10^{-4} and v_p decreases by 70 km s^{-1}. We combine these in quadrature with the changes that resulted from scaling the dust at the 68% level and adopt the total as the systematic uncertainty due to dust contamination.

Temperature fluctuations in the CMB are a potential source of confusion for SZE measurements. Measurements of the kinetic SZE are particularly susceptible since the spectral dependence of the kinetic SZE and CMB fluctuations are identical, absent relativistic corrections to the SZE at the few percent level. Recent BIMA observations at 28.5 GHz have provided good constraints on CMB anisotropy at the angular scales of our measurement (Dawson et al. 2001; Holzapfel et al. 2000); they find $\Delta I_\nu < 4.8 \times 10^{-4}$ MJy sr^{-1} at 95% confidence, which is just 1% of ΔI_{30}. This uncertainty is negligible given the precision of our measurement. The level of CMB contamination may be larger in the SuZIE bands, however, particularly near the null in the thermal SZE.

To test the level of CMB contamination in the SuZIE bands we first use the software package CMBfast (Zaldarriaga & Seljak 2000) to generate a CMB power spectrum up to a multipole $\ell =$ 2500. We assume a universe consisting of cold dark matter with a cosmological constant (ΛCDM) and use conventional parameter values $(\Omega_b, \Omega_{cdm}, \Omega_\Lambda, \tau_c, n_s, h) = (0.04, 0.26, 0.70, 0, 0.95, 0.72)$ where Ω_b is the fractional baryon density of the universe, Ω_{cdm} is the fractional cold dark matter density, Ω_Λ is the fractional density of vacuum energy, τ_s is the optical depth to reionization, n_s is the spectral index of the power spectrum, and $H_0 = 100h$ km s^{-1} Mpc^{-1} is the Hubble constant. The values chosen are good estimates given the range of values currently constrained by CMB anisotropy measurements (Pryke et al. 2001; Netterfield et al. 2001; Stompor et al. 2001); h comes from the Hubble Space Telescope Hubble Constant key project (Freedman et al. 2001). To account for secondary anisotropies we conservatively assume a flat power spectrum for $\ell > 2500$, corresponding to arcminute angular scales. The flat band power we use corresponds to $\Delta T_{\rm CMB}/T_{\rm CMB} \sim 5 \times 10^{-6}$, which is consistent with expectations of secondary anisotropies (Hu & Dodelson 2001) and the BIMA limit of Dawson et al. (2001). We then use this power spectrum to produce mock CMB fields at SuZIE's resolution. After simulating the SuZIE scan on these maps, we fit them to an isothermal β-model and use a Monte Carlo procedure similar to that used with the dust to determine the contribution of CMB to the total signal in each SuZIE band. Upon fitting to 10^4 different maps for each band, we find an rms of ± 0.020 MJy sr^{-1} at 1.1 mm, ± 0.022 MJy sr^{-1} at 1.4 mm, and ± 0.017 MJy sr^{-1} at 2.1 mm. Further tests using only primary anisotropy ($\ell \lesssim 2500$) or only secondary anisotropy ($\ell \gtrsim 2500$) indicate that primary anisotropy is responsible for roughly 80% of the total CMB contribution in all three bands. Including the rms total anisotropy contributions in the SuZIE signals listed in Table 1, we redo the spectral fit and find changes of ± 0.05 in y_0 and $^{+420}_{-400}$ km s^{-1} in v_p. The peculiar velocity suffers more from confusion with CMB anisotropy than does the Compton y-parameter, as anticipated. We adopt these results as the systematic uncertainties due to CMB contamination.

We also consider confusion with extended emission from the radio halo surrounding Abell 2163, which is the brightest such halo yet discovered (Feretti et al. 2001). To test its effect on the 1 cm decrement, we combine the OVRO data with the 1.4 cm NVSS map of the cluster region, which shows a large region of extended emission surrounding the cluster. We first scale the NVSS map to account for the unknown spectrum of the radio halo; we make this scale factor a free parameter and redo the fit described in §2. The decrement is increased by -0.003 MJy sr^{-1} when we include this extra parameter, and the scaling is consistent with a spectral index $\alpha \simeq 1.2$ where the intensity has a $\nu^{-\alpha}$ dependence. We note, however, that our fit is consistent with $\alpha = \infty$ (i.e., no radio halo) within 68% confidence. Furthermore, the spectral index may not be constant across the halo, so the best-fit α must be taken as a crude estimate. H1997b also address radio halo confusion, and estimate a 2% effect at 2.1 mm. This assumes a spectral index of ~ 1.5, however; using our best-fit value $\alpha = 1.2$, the effect increases to $\sim 5\%$. When we alter the 1 cm and 2.1 mm points accordingly and redo the spectral fit, we find that y_0 increases by 0.17×10^{-4} to 3.73×10^{-4}, and v_p increases by 50 km s^{-1} to 460 km s^{-1}. We adopt these as estimates of the systematic uncertainties in y_0 and v_p due to radio halo confusion.

We use a similar treatment to determine the systematic uncertainty due to point source contamination. In §2 we accounted for the possibility of an undetected on-center point source in the field at 1 cm, and found that it could increase the magnitude of the measured decrement by 0.001 MJy sr^{-1}. Such a faint source would not affect the SuZIE data unless it had a strongly inverted spectrum; we assume that it does not. The brighter off-center point source detected at 1 cm could affect the SuZIE data if its spectrum were inverted at millimeter wavelengths. Although its flux rises from 1 to 3 mJy between 6 cm and 2 cm (M. Birkinshaw 2001, private communication), we found at the time of our observations that the flux of the source at 1 cm varied between 1.1 and 1.4 mJy. This corresponds to a spectral index α between 1.1 and 1.5. Extrapolating with such a spectral index to 2.1 mm, we find a flux of less than 0.2 mJy which would have a negligible effect on the decrement. However, because of its variability and unusual spectrum, we conservatively assume a flat spectral index ($\alpha = 0$) for $\lambda < 1$ cm. Changing the 1 cm decrement to account for a faint central point source and altering the SuZIE 2.1 mm decrement to account for a 1.5 mJy point source, we find an increase of 0.07×10^{-4} in y_0 and 50 km s^{-1} in v_p. We include these in Table 3 as our systematic uncertainty due to point source contamination.

We test the importance of our assumed 12.4 keV electron temperature to y_0 and v_p by performing the spectral fit over a large range in T_e. An increase in T_e trades off with a decrease in the cluster optical depth $\tau = \int n_e \sigma_T dl$, as can be seen in equation (7); thus so long as τ remains a free parameter, Compton y is only weakly sensitive to temperature changes. In the 1σ range of T_e (10.5 keV $\leq T_{\rm e} \leq$ 15.2 keV), y_0 varies by $^{+0.09}_{-0.07} \times 10^{-4}$. The peculiar velocity also has a weak temperature dependence; it rises with temperature at low $T_{\rm e}$ ($\lesssim$ 5 keV) as τ decreases (cf. equation 8), then falls at high T_e ($\gtrsim$ 15 keV) due to relativistic corrections. The 1σ range of T_e corresponds to a broad plateau in the T_e-v_p curve, and we find v_p varying by only +20 km s^{-1} and -40 km s^{-1}.

We have assumed an isothermal temperature distribution for the cluster gas, consistent with the H1997a and b treatments of Abell 2163. Although the assumed cluster temperature has little impact on y_0 and v_p, uncertainties in the thermal structure of the cluster may have a larger effect. In a recent study of Abell 2163 using the *BeppoSAX* X-ray satellite, Irwin & Bregman (2000) find the cluster temperature profile consistent with isothermality at the 2σ confidence level out to a radius of $9'$; this is consistent with the result of White (2000), who finds a temperature profile consistent with isothermality at the 1σ confidence level out to $10'$. Chandra or XMM data are necessary to place stronger constraints on the thermal profile of Abell 2163, and we postpone quantifying a systematic uncertainty until such data become available.

Finally, we consider the effect of the assumed $\pm 8\%$ absolute calibration uncertainty in each SuZIE band and the $\pm 3\%$ absolute calibration uncertainty in our interferometric 1 cm measurements. These combine to change y_0 by as much as $\pm 0.17 \times 10^{-4}$ and v_p by up to ± 170 km s^{-1}.

4. CONCLUSIONS

We have used interferometric data obtained at the OVRO and BIMA observatories to determine the SZE intensity decrement in the cluster Abell 2163 at a wavelength of 1 cm. We find $\Delta I_{30} = -0.048 \pm 0.006$ MJy sr^{-1} by modeling the ICM as an isothermal spherical β-model. We have thus expanded the spectral coverage of this cluster to include the Rayleigh-Jeans part of the CMB blackbody spectrum and we present the most complete SZE spectrum to date. Upon fitting the OVRO/BIMA and SuZIE data for Abell 2163 to an SZE spectral model, we find $y_0 = 3.56^{+0.41+0.27}_{-0.41-0.19} \times 10^{-4}$ and $v_p = 410^{+1030+460}_{-850\ -440}$ km s^{-1} where we list statistical uncertainty followed by systematic uncertainty at 68% confidence. The systematic uncertainties in Table 3 have been combined in quadrature to determine the totals reported above. We have shown that adding the 1 cm measurement improves constraints on the Compton y-parameter, as expected, but has less effect on the peculiar velocity which is best constrained by measurements near the 218 GHz thermal null.

The spectral fit includes corrections for dust emission in the SuZIE bands; we find that the contamination level depends strongly on the observing scheme of the instrument due to the distribution of dust on the sky. The dust contamination level for a cluster will obviously depend on its location on the sky; the line of sight to Abell 2163 passes near the Galactic plane, so it is more susceptible to dust contamination than clusters at higher galactic latitudes.

Finally, we emphasize that the Abell 2163 spectrum shown in Figure 2 consists of data from two very different experiments; an array of six bolometers performing drift scans (SuZIE) and two interferometers (OVRO and BIMA). The remarkable consistency that we find amongst the two sets of measurements is further evidence that SZE observations are now a reliable probe of structure in the universe.

This work is supported by NASA LTSA grant NAG5–7986. Many thanks to Erik Leitch for the use of his CMB field-generating software and for many helpful discussions. Thanks also to Amber Miller for useful discussions and much help with point sources. Clem Pryke provided invaluable information on the flux distribution of point sources detected by the DASI experiment. We thank the staff of the OVRO and BIMA observatories for their support and hard work, in particular J. R. Forster, J. Lugten, S. Padin, R. Plambeck, S. Scott, and D. Woody. Radio astronomy at the BIMA millimeter array is supported by NSF grant AST 96–13998, and the OVRO millimeter array is supported by NSF grant AST 96–13717. E. R. acknowledges support from NASA GSRP Fellowship NGT5–50173, and J. C. acknowledges support from a NSF–YI grant and the David and Lucile Packard Foundation. The Digitized Sky Survey was produced at the Space Telescope Science Institute under U.S. Government grant NAG W-2166. The images of these surveys are based on photographic data obtained using the Oschin Schmidt Telescope on Palomar Mountain and the UK Schmidt Telescope. The plates were processed into the present compressed digital form with the permission of these institutions. We thank S. Hansen, S. Pastor, and D. Semikoz for politely pointing out an error in our initial spectral fit. Finally, we thank M. Birkinshaw and M. Giard for the useful information they have provided.

REFERENCES

Beichman, C. A., Neugebauer, G., Habing, H. J., Clegg, P. E., & Chester, T. J. 1988, NASA Reference Publication, 1190, 1

Carlstrom, J. E., Joy, M., & Grego, L. E. 1996, ApJ, 456, L75

Cavaliere, A. & Fusco-Femiano, R. 1978, A&A, 70, 677

Condon, J. J., Cotton, W. D., Greisen, E. W., Yin, Q. F., Perley, R. A., Taylor, G. B., & Broderick, J. J. 1998, AJ, 115, 1693

Dawson, K. S., Holzapfel, W. L., Carlstrom, J. E., Joy, M., LaRoque, S. J., & Reese, E. D. 2001, ApJL–submitted: astro-ph/0012151

Desert, F. ., Benoit, A., Gaertner, S., Bernard, J. ., Coron, N., Delabrouille, J., de Marcillac, P., Giard, M., Lamarre, J. ., Lefloch, B., Puget, J. ., & Sirbi, A. 1998, New Astronomy, 3, 655

Feretti, L., Fusco-Femiano, R., Giovannini, G., & Govoni, F. 2001, A&A, 373, 106

Finkbeiner, D. P., Davis, M., & Schlegel, D. J. 1999, ApJ, 524, 867

Fixsen, D. J., Cheng, E. S., Gales, J. M., Mather, J. C., Shafer, R. A., & Wright, E. L. 1996, ApJ, 473, 576

Freedman, W. L., Madore, B. F., Gibson, B. K., Ferrarese, L., Kelson, D. D., Sakai, S., Mould, J. R., Kennicutt, R. C., Ford, H. C., Graham, J. A., Huchra, J. P., Hughes, S. M. G., Illingworth, G. D., Macri, L. M., & Stetson, P. B. 2001, ApJ, 553, 47

Grego, L., Carlstrom, J. E., Joy, M. K., Reese, E. D., Holder, G. P., Patel, S., Cooray, A. R., & Holzapfel, W. L. 2000, ApJ, 539, 39

Holzapfel, W. L., Ade, P. A. R., Church, S. E., Mauskopf, P. D., Rephaeli, Y., Wilbanks, T. M., & Lange, A. E. 1997a, ApJ, 481, 35

Holzapfel, W. L., Arnaud, M., Ade, P. A. R., Church, S. E., Fischer, M. L., Mauskopf, P. D., Rephaeli, Y., Wilbanks, T. M., , & E., L. A. 1997b, ApJ, 480, 449

Holzapfel, W. L., Carlstrom, J. E., Grego, L., Holder, G., Joy, M., & Reese, E. D. 2000, ApJ, 539, 57

Hu, W. & Dodelson, S. 2001, in 52 pages, 5 figures, 5 plates; Ann. Rev. Astron. Astrophys. 2002 http://background.uchicago.edu/ whu, 10414

Irwin, J. A. & Bregman, J. N. 2000, ApJ, 538, 543

Itoh, N., Kohyama, Y., & Nozawa, S. 1998, ApJ, 502, 7

Lamarre, J. M., Giard, M., Pointecouteau, E., Bernard, J. P., Serra, G., Pajot, F., Désert, F. X., Ristorcelli, I., Torre, J. P., Church, S., Coron, N., Puget, J. L., & Bock, J. J. 1998, ApJ, 507, L5

Netterfield, C. B., Ade, P. A. R., Bock, J. J., Bond, J. R., Borrill, J., Boscaleri, A., Coble, K., Contaldi, C. R., Crill, B. P., de Bernardis, P., Farese, P., Ganga, K., Giacometti, M., Hivon, E., Hristov, V. V., Iacoangeli, A., Jaffe, A. H., Jones, W. C., Lange, A. E., Martinis, L., Masi, S., Mason, P., Mauskopf, P. D., Melchiorri, A., Montroy, T., Pascale, E., Piacentini, F., Pogosyan, D., Pongetti, F., Prunet, S., Romeo, G., Ruhl, J. E., & Scaramuzzi, F. 2001, "submitted: ApJ", 4460+, astro-ph/0104460

Nozawa, S., Itoh, N., & Kohyama, Y. 1998, ApJ, 508, 17

Pearson, T. J., Shepherd, M. C., Taylor, G. B., & Myers, S. T. 1994, in American Astronomical Society Meeting, Vol. 185, 0808

Pospieszalski, M. W., Lakatosh, W. J., Nguyen, L. D., Lui, M., Liu, T., Le, M., Thompson, M. A., & Delaney, M. J. 1995, IEEE MTT-S Int. Microwave Symp., 1121

Pryke, C., Halverson, N. W., Leitch, E. M., Kovac, J., Carlstrom, J. E., Holzapfel, W. L., & Dragovan, M. 2001, ApJ–submitted: astro-ph/0104490

Sault, R. J., Teuben, P. J., & Wright, M. C. H. 1995, in ASP Conf. Ser. 77: Astronomical Data Analysis Software and Systems IV, Vol. 4, 433

Scoville, N. Z., Carlstrom, J. E., Chandler, C. J., Phillips, J. A., Scott, S. L., Tilanus, R. P. J., & Wang, Z. 1993, PASP, 105, 1482

Serra, G. et al. 1998, in Proc. ICSO Conf., Toulouse, Poster Session 2

Stompor, R., Abroe, M., Ade, P., Balbi, A., Barbosa, D., Bock, J., Borrill, J., Boscaleri, A., de Bernardis, P., Ferreira, P. G., Hanany, S., Hristov, V., Jaffe, A. H., Lee, A. T., Pascale, E., Rabii, B., Richards, P. L., Smoot, G. F., Winant, C. D., & Wu, J. H. P. 2001, ApJ, 561, L7

Sunyaev, R. & Zel'dovich, Y. 1972, Comments Astrophys. Space Phys., 4, 173

White, D. A. 2000, MNRAS, 312, 663

Zaldarriaga, M. & Seljak, U. 2000, ApJS, 129, 431

This preprint was prepared with the AAS LaTeX macros v5.0.

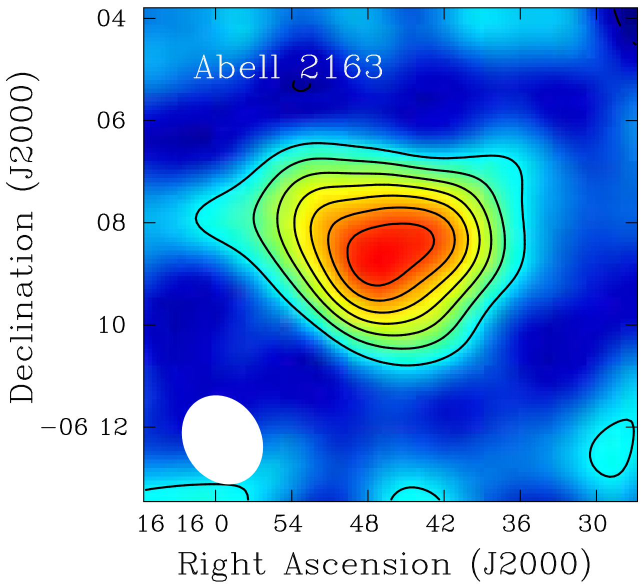

Fig. 1.— Deconvolved 1 cm SZE image for Abell 2163, constructed from BIMA data. The image was made by first applying a Gaussian taper to the u-v data with a half power radius of 1.5 kλ; the resulting beam FWHM ($110'' \times 90''$ at position angle 30°) is shown by the white ellipse in the lower left. The rms is 300 μJy beam^{-1}, corresponding to a Rayleigh Jeans brightness sensitivity of 50 μK. Contours are integer multiples of $\pm 1.5\sigma$ with negative contours shown as solid lines.

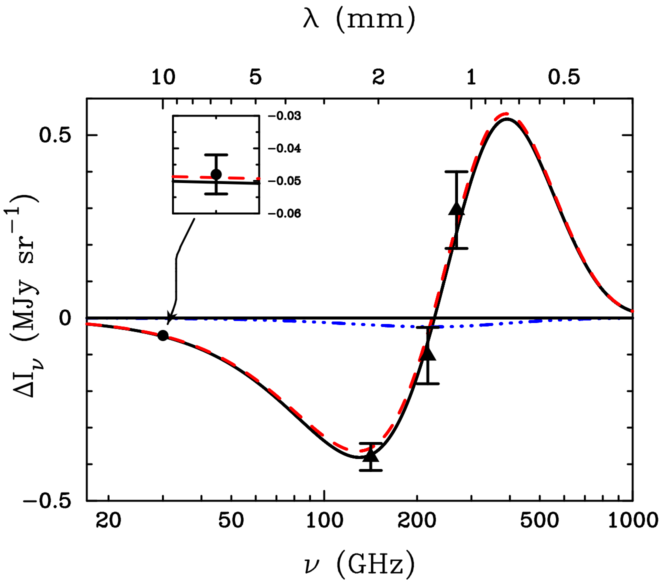

Fig. 2.— SZE spectrum of Abell 2163 (points) and best fit model (lines). The dashed line is the thermal spectrum, dot-dashed the kinetic spectrum, and solid the sum of the two; SuZIE data points appear as triangles and OVRO & BIMA as a circle. The insert shows the 1 cm point with its error bar.

Table 1. Measurements of SZE in Abell 2163

λ (mm)	Instrument	Measured $\Delta I_{\nu 0}$ (MJy sr^{-1})	Dust-corrected $\Delta I_{\nu 0}$ (MJy sr^{-1})
10.0	OVRO & BIMA	-0.048 ± 0.006	...
2.1	Diabolo	-0.545 ± 0.22	...
2.1	SuZIE	-0.381 ± 0.037	-0.380 ± 0.037
1.4	SuZIE	-0.106 ± 0.077	-0.103 ± 0.077
1.1	SuZIE	0.287 ± 0.105	0.295 ± 0.105

Table 2. Strength of Dust Signals

Map (μm)	$\Delta I_{\nu 0}$ (MJy sr^{-1})
1100	$-7.6^{+1.2}_{-1.4} \times 10^{-3}$
1400	$-3.5^{+0.5}_{-0.6} \times 10^{-3}$
2100	$-0.7^{+0.1}_{-0.1} \times 10^{-3}$

Table 3. Systematic Uncertainties in y_0 and v_p

Source	Effect on y_0 ($\times 10^{-4}$)	Effect on v_p (km s^{-1})
Dust Contamination	$(+0.02, -0.01)$	$(+30, -70)$
CMB Anisotropy	$(+0.05, -0.05)$	$(+420, -400)$
Radio Halo	$(+0.17, -0)$	$(+50, 0)$
Point Sources	$(+0.07, -0)$	$(+50, -0)$
X-ray Temperature	$(+0.09, -0.07)$	$(+20, -40)$
Absolute Calibration	$(+0.17, -0.17)$	$(+170, -170)$
Total[a]	$(+0.27, -0.19)$	$(+460, -440)$

[a]combined in quadrature.